Investigating the Impact of Aerosol Deposition on Snow Melt over the Greenland Ice Sheet Using a Large-Ensemble Kernel

Yang Li[1], Mark G. Flanner[1]

[1] Climate and Space Sciences and Engineering, University of Michigan, Ann Arbor, Michigan, USA

Correspondence to: Y. Li, yanglibj@umich.edu

Abstract

Accelerating surface melt on the Greenland Ice Sheet (GrIS) has led to a doubling of Greenland's contribution to global sea level rise during recent decades. Black carbon (BC), dust, and other light absorbing impurities (LAI) darken the surface and enhance snow melt by boosting the absorption of solar energy. It is therefore important for coupled aerosol-climate and ice sheet models to include snow darkening effects from LAI, and yet most do not. In this study, we conduct several thousand simulations with the Community Land Model (CLM) component of the Community Earth System Model (CESM) to characterize changes in melt runoff due to variations in the amount, timing, and nature (wet or dry) of BC deposition on the GrIS. From this large matrix of simulations, we develop a kernel relating runoff to the location, month, year (from 2006-2015), and magnitudes of BC concentration within precipitation and dry deposition flux. BC deposition during June-August causes the largest increase in annually-integrated runoff, but winter deposition

events also exert large (roughly half as great) runoff perturbations due to re-exposure of impurities at the snow surface during summer melt. Current BC deposition fluxes simulated with the atmosphere component of CESM induce a climatological-mean increase in GrIS-wide runoff of ~8 Gt/yr, or +6.8% relative to a paired simulation without BC deposition. We also provide linear equations that relate the increase in total runoff to GrIS-wide wet and dry BC deposition fluxes. It is our hope that the runoff kernel and simple equations provided here can be used to extend the utility of state-of-the-art aerosol models.

1 Introduction

The Greenland Ice Sheet (GrIS) holds the equivalent of about 7 m of sea level rise (Kintisch, 2017). During recent decades, the accelerating decline of the GrIS has doubled Greenland's contribution to global sea level rise to about 0.74 mm per year (Shepherd et al., 2012; Rignot and Kanagaratnam, 2006; van den Broeke et al., 2009; Kintisch, 2017). Mass loss from the GrIS is predicted to raise sea level by more than 20 cm by 2100 (Rignot et al., 2011; Dumont et al., 2014), imposing tremendous effects on global society.

Ice loss from the GrIS is caused by many physical and biological factors, including: 1) increase of air temperature over the Arctic region, which accelerates surface melting; 2) declining surface albedo, which can be caused by a variety of effects including increased melt area, enhanced snow metamorphism, and accumulation of light-absorbing impurities (LAI) (Tedesco et al., 2016; Box et al., 2012; Dumont et al., 2014; Keegan et al., 2014; Shimada et al., 2016; Polashenski et al., 2015); and 3) calving of icebergs and submarine melting due to ice dynamics and changes of ocean temperature (Krabill et al., 2004; Zwally et al., 2002; Dumont et al., 2014). Since 2005, surface melting has likely contributed more to ice loss than iceberg calving (Kintisch, 2017). Sources of LAI include black carbon (BC), mineral dust, and algae and bacteria growing on the wet surface of the ice sheet, all of which darken the surface, boost the absorption of insolation and enhance snow melt.

BC is a major anthropogenic pollutant originating from fossil fuel combustion, open biomass burning, and biofuel use, and is a key LAI because its solar

53 absorptivity is extremely high (e.g., Bond et al., 2013). Previous climate modeling
54 studies simulate annual warming in the Arctic region with the inclusion of BC in
55 snow (Flanner et al., 2007; Flanner et al., 2009; Hansen and Nazarenko, 2004;
56 Hansen et al., 2005; Jacobson, 2004), and find BC/snow forcing induces a global
57 temperature response about three times greater than equal forcing from CO_2
58 (Flanner et al., 2007). BC influences snow coverage by warming the atmosphere,
59 reducing surface insolation through "dimming", and reducing snow reflectance
60 through darkening caused by BC deposition to snow surface. Globally, the darkening
61 effect within snow increases solar heating of snowpack, and exceeds the loss of
62 absorbed energy from dimming, causing a positive net surface forcing and
63 snowpack melting (Flanner et al., 2009). Melting snow also tends to retain BC
64 aerosols, which darken the surface more and increase absorption of insolation (e.g.,
65 Doherty et al., 2013). Therefore, it is important for coupled aerosol-climate and ice
66 sheet models to include BC darkening effects, and yet most do not.
67 Global BC emissions from fossil fuel and biofuel combustion have increased
68 dramatically during the industrial era. Since the early 20th century, BC emissions
69 also shifted spatially, decreasing in North American and Europe but increasing in
70 Asia (Bond et al., 2007; Bond et al., 2013). Both the spatial pattern of emissions and
71 the circulation features that are coincident with emissions can strongly effect the
72 amount of BC reaching the Arctic and depositing to the GrIS (Doherty et al., 2010;
73 Thomas et al., 2017; Jiao et al., 2014).
74 In this study, we develop a BC deposition-snow melt kernel using the
75 Community Earth System Model (CESM) to investigate changes in snow melt and

surface runoff due to variations in the amount and timing of aerosol deposition on the GrIS. More than 5000 simulations are conducted with the Community Land Model (CLM) component of CESM, driven with a large range of wet and dry BC deposition fluxes to determine relationships between snow melt perturbation and deposition amount occurring in different months. The final kernel product is resolved by type of BC deposition (wet or dry), deposition amount, deposition month, and deposition year ranging from 2006-2015. It is our hope that this kernel will benefit regional and global aerosol modeling communities by allowing them to estimate GrIS snow melt and surface runoff perturbations associated with different aerosol deposition fluxes.

2 Methods

2.1 Simulation design

We use the Community Earth System Model (CESM) version 1.2.2, and run the offline Community Land Model (CLM) (Oleson et al., 2013) version 4.5 with prescribed wet or dry BC deposition in the snow sub-model to study the effects of BC deposition on snow melt and runoff from Greenland. Our motivation for using CLM in this offline configuration is that (1) it reduces noise associated with ocean and atmosphere variability, enabling clearer identification of the runoff signal caused by snow perturbations, and (2) the simulations are computationally cheap, allowing us to explore a large parameter space. We drive the simulations using meteorological forcing data from the Climatic Research Unit and National Centers for Environmental Prediction (CRUNCEP) (Viovy, 2012) over the period 2006-2016.

98 CRUNCEP data cover the global land surface at a spatial resolution of a 0.5° × 0.5°,
99 and are provided with relatively low latency, allowing us to explore conditions over
100 the recent past. In CLM, the representation of terrestrial snow, including over ice
101 sheets, is based loosely on the SNTHERM model (Jordan, 1991) and is described in
102 detail by Oleson et al., 2013. Snow albedo and solar absorption within each snow
103 layer are simulated with the Snow, Ice, and Aerosol Radiative Model (SNICAR),
104 which accounts for solar zenith angle, albedo of the substrate underlying snow,
105 mass concentrations of LAI (black carbon, dust, organic carbon, and volcanic ash),
106 and ice effective grain size. In general, CLM/SNICAR represents five vertical snow
107 layers, and accounts for variations in LAI concentration due to dry and wet
108 deposition, particle flushing and retention with melt water, snow sublimation, and
109 layer combinations and divisions (Oleson et al., 2013). Dry BC deposition from the
110 atmosphere occurs through gravitational settling and turbulent mixing, primarily
111 transferring hydrophobic BC to the surface, while wet BC deposition occurs via
112 precipitation and only affects hydrophilic BC in the model. CLM maintains mass
113 burdens of both hydrophilic BC and hydrophobic BC within each snow layer, with
114 each species having unique optical properties and meltwater removal efficiencies.
115 Deposited particles are assumed to be instantly mixed and homogeneous within the
116 surface snow layer, which does not exceed 2 cm in thickness. The particles are
117 added after the computation of inter-layer water fluxes, thus preventing particles in
118 the top layer from being washed out immediately before radiative calculations.
119 Particle masses are redistributed vertically in each time step proportionately with
120 snow melt through the snow column, scaled by the species-specific melt scavenging

efficiency, and snow layer combination and subdivision. The masses carried out with meltwater drainage through the bottom snow layer are permanently lost from the snowpack, and are not maintained within the model (Oleson et al., 2013).

For each simulation used to generate the kernel relating melt runoff to BC deposition, we prescribe uniform concentrations of BC within precipitation or uniform dry deposition fluxes over the ice sheet for a period of one month, and quantify perturbations to snow and melt runoff for one year or more following the period of deposition. 23 unique BC concentrations in precipitation (e.g., snow) are prescribed to provide wet BC flux in the CLM. We use a wide range of wet BC concentrations (from 1 ng g^{-1} ~ 500 ng g^{-1}) with logarithmic spacing, aiming to cover historically observed BC concentrations over the Greenland region (Figure 1) and potential severe episodes associated (e.g.,) with extreme fire activity. For example, measured values of BC in Greenland snow during 2012-2014, collected from snow pits across a long transect, averaged 2.6 ng g^{-1} (Polashenski et al., 2015). Peak values throughout the depth of the snow pits averaged 4 ng g^{-1} and 15 ng g^{-1} in 2012 and 2013, respectively, and the largest single measurement was 43 ng g^{-1}. Ice core measurements from D4 dating back to 1788 show annual-mean concentrations peaking in the early 20th century at ~12.5 ng g^{-1}, mean concentrations of 2.3 ng g^{-1} during 1952-2002, and occasional monthly-mean peaks exceeding 50 ng g^{-1} due to biomass burning events (McConnell et al., 2007). Correspondingly, the maximum dry BC deposition flux is calculated as the product of the maximum wet BC concentration (500 ng g^{-1}) and the mean monthly snowfall (1.75×10^{-5} mm s^{-1}) over an 11-year (2006-2016) CESM simulation. We prescribe 24

144 unique dry BC fluxes (0.01 ng m^{-2} s^{-1}-8.80 ng m^{-2} s^{-1}) with logarithmic spacing in our
145 study (Figure 1).

146 With each prescribed BC deposition value, we perform 12 simulations with
147 specified BC deposition month from January to December in each deposition year.
148 Each simulation starts from January in the deposition year, and extends to one full
149 year after the deposition month in order to study the annually integrated BC effects.
150 We then repeat these simulations for ten years (2006-2015) to generate a
151 climatological product and explore the magnitude of interannual variability in melt
152 perturbations due, for example, to differences in precipitation and near-surface air
153 temperatures. In summary, we perform 2,760 simulations (23 wet BC
154 concentrations × 12 deposition months × 10 deposition years) to study the effects of
155 wet BC deposition, and 2,880 simulations (24 dry BC fluxes × 12 deposition months
156 × 10 deposition years) to study the effects of dry BC deposition. 120 simulations (12
157 deposition months × 10 deposition years) without BC deposition are also performed
158 as parallel control/base runs from which to derive the perturbations induced by BC
159 deposition. The timestep of CLM/SNICAR for our simulations is 0.5 hour, and the
160 spatial resolution is 0.9° x 1.25°. The kernel product is calculated as monthly mean
161 values with the same spatial resolution.

162 **2.2 Simulation length evaluation based on top-snow layer BC concentration**

163 To evaluate the importance of simulation length for the purposes outlined, we
164 focus on BC concentration in the top snow layer because properties of this layer
165 dominate the bulk solar radiative properties of the snowpack. In Figure 2, we
166 examine the mean distribution of BC concentration in the top snow layer over

167 Greenland after maximum wet and dry BC deposition fluxes occur in January and
168 June. These contours are averaged over ten years to show a climatological state.
169 Top-layer BC concentrations after wet BC deposition show higher values in the
170 center and south margin of Greenland (Figure 2a, b, e, f), which matches the general
171 precipitation pattern over the GrIS, with elevated precipitation amount in the center
172 and south of GrIS. Meanwhile, higher top-layer BC values occur over the north of
173 Greenland after dry BC deposition (Figure 2c, d, g, h), as lower precipitation in these
174 regions enhances the effect of dry deposition. Also, we find lower concentrations
175 induced by the maximum wet BC (Figure 2a, b, e, f) than by the maximum dry BC
176 deposition (Figure 2c, d, g, h). Top-layer BC concentration decreases rapidly only
177 one month after the deposition month for both winter and summer deposition (i.e.,
178 from January to February with January deposition in Figure 2a-d, and from June to
179 July with June deposition in Figure 2e-h), as new snowfall dilutes the contaminated
180 snow. The rapid decrease in BC concentration supports the notion that a one-year
181 simulation length should capture most of the time-integrated effect from a
182 deposition event. To verify this, we also perform two 11-year (2006-2016)
183 simulations with the maximum wet BC deposition occurring in April and October of
184 the first year, to evaluate the long-term variation of top-layer BC concentration. In
185 these long-term simulations, we find top-layer BC concentrations decrease rapidly
186 within a one-year period after both spring and fall depositions (Figure 3). We also
187 see, however, that residual BC reappears at the surface in subsequent summers
188 because of snow melting and associated accumulation of impurities at the top of the
189 snowpack (Doherty et al., 2013). In the model, this occurs because melt scavenging

ratios for both types of BC are less than 1, meaning that proportionately less BC moves down vertically in the column than meltwater. As we will see, summer re-appearance of impurities at the snow top has a non-negligible impact on the annually-integrated runoff perturbation, but the peaks in subsequent years are less than 1/20 of the BC concentrations in the deposition month, indicating that the one-year simulation setup is reasonable to capture the major portion of the total BC influences.

3 Results and Discussion

Deposited BC to snow causes a darkening effect and enhances snow melt and Greenland runoff. Here, we first show variations of top-snow layer BC concentrations, and then examine total GrIS runoff perturbation induced by BC deposition.

3.1 BC concentration in the top snow layer

We investigate the climatological (i.e., averaged over ten simulations covering 2006-2015) 1-year evolution of top-snow layer BC concentration averaged over Greenland for different deposition months. Figure 4 depicts the temporal evolution of top-layer BC concentration for the maximum wet and dry BC fluxes from our matrix of simulations. For all months of deposition, top-layer concentrations decrease rapidly as fresh snow covers the contaminated surface. Top-snow layer concentrations of dry-deposited BC generally decrease more slowly than those of wet-deposited BC. One reason for this behavior during summer months is that dry-deposited BC is assumed to be hydrophobic and have a lower meltwater scavenging

efficiency, reducing the rate at which it is carried away by melting water. We also see, however, that some winter-deposited BC can persist in the top layer until, or even re-appear during, the summer melt season, indicating that BC deposition in non-melting seasons can also be important for GrIS melting. Re-exposure of previously deposited BC occurs as overlying snow melts and flushes through the snow, removing some but not all of the underlying impurities and eventually exposing the dirty snow layer at the surface.

We also investigate how top-layer BC concentration varies with different BC deposition values, and how this variation evolves over one year following deposition (Figure 5 and Figure 6). For all deposition months, top-snow layer BC concentration increases, as expected, with increasing BC deposition flux. The relationship between top-layer BC concentration and BC deposition value is nearly linear, although we find indications of saturation at later times with dry BC deposition (e.g., as in Figure 6h-l). Figure 7 summarizes top-layer BC concentration variation with deposition amount at different times (0-11 months since deposition) averaged over all the deposition months. With this averaging, we find that top-layer BC concentrations decrease monotonically from month 0 to month 11. Again, we find slower decrease in the dry deposition simulations than in the wet deposition simulations. With wet BC deposition, the rate of decrease slows down after 3-6 months, which could be due to the summer peaks resulting from snow melting and BC integration (Figure 4).

3.2 Temporal variation of GrIS total runoff

We define total runoff in CLM as the summation of surface runoff, sub-surface

drainage and runoff from glacier surface. We first examine the seasonal and inter-annual variation of GrIS total runoff, integrated over the entire GrIS, in the base run without BC deposition (Figure 8). Total runoff shows clear summer peaks and some inter-annual variation. Annual-integrated total runoff is ~120 Gt per year, with the highest value of ~140 Gt in 2014 (Figure 8b). Compared with satellite gravity measurements during 2005-2010 showing Greenland is losing mass at a rate of ~229 Gt/yr (169-290 Gt/yr), of which 50-70% is lost through surface melt (Vaughan et al., 2013), the simulated total runoff in the base run in our study is within a reasonable range.

We then calculate perturbed total runoff due to BC deposition as the difference in runoff between simulations with BC deposition and paired base simulations without BC deposition. We select three wet BC deposition values and three dry BC deposition values to illustrate the seasonal and inter-annual variations of perturbed total runoff (Figure 9). We note that different scales are used in the panels of Figure 9, which shows that higher deposition causes more total runoff. We also find clear inter-annual variations for different deposition amounts and months. The variations of perturbed total runoff in Figure 9 follow the variation of total runoff in the base run (Figure 8) in general, especially for the perturbed simulations with wet BC depositions, indicating that BC deposition could have greater effect in warmer years, when more of the ice sheet is near the melting temperature. This could also be due to an amplification effect by metamorphism of snow in warmer years.

To remove the effect of yearly variation, we also investigate the climatological (i.e., averaged over ten simulations spanning 2006-2015) 1-year evolution of total

runoff increase due to BC deposition starting from different deposition months. Again, we examine total runoff increase induced by maximum wet and dry BC depositions to understand general behavior associated with very large perturbations, for which the signal is much larger than noise. As shown in Figure 10, we find two summer peaks of total runoff increase, with the second peak caused by the re-exposure of BC during the summer after deposition. We also find total runoff perturbation is the largest in July for all months of deposition, followed by August. The largest perturbation in summer could be caused by immediate melting due to darkening, as well as larger grain size in warmer environment.

3.3 GrIS total runoff variation with deposition amount

As represented by Figure 9, higher deposition amount causes larger total runoff increase. Here, we examine total runoff perturbation caused by all deposition amounts, and how total runoff distributes over Greenland. Figure 11 and Figure 12 show climatological mean (2006-2015) annually integrated total runoff increase caused by June BC deposition via wet and dry processes, respectively. June deposition is selected for these figures because of its high potential to impact summer melt. Although BC is well distributed over the whole GrIS (Figure 2), total runoff perturbations are largely confined to the low elevation margins with both wet and dry BC deposition (Figure 11 and Figure 12), as these remain the only areas warm enough in the model simulations for substantial melt to occur, which is consistent with the Tedesco, 2007 study. We note that the spatial distribution of model melt will be sensitive to surface air temperature and insolation, the latter of which can vary substantially between re-analysis products. Runoff effects of dry BC

281 deposition show similar patterns as impacts from BC in precipitation. We find that
282 small fluxes of BC via dry deposition are not as effective as similar deposition fluxes
283 of BC in precipitation, and we attribute this to the higher light absorptivity (and
284 hence radiative forcing per unit mass) of hydrophilic BC than of hydrophobic BC.
285 The former is assumed to be coated with non-absorbing sulfate and hence its mass
286 absorption cross-section is about 50% larger than that of uncoated hydrophobic BC
287 (Flanner et al., 2007).

288 Figure 13 summarizes the variation of total runoff perturbation versus
289 deposition amount for different deposition months. The maximum BC deposition
290 perturbs total runoff by up to ~20% (24 Gt) in the wet BC deposition simulations,
291 although we note that continent-wide fluxes of this magnitude (500 ng g^{-1} in
292 precipitation) are much larger than ever observed on Greenland. With a modest
293 deposition concentration (e.g., 5 ng/g), the runoff perturbation is ~0.4% (~0.5 Gt).
294 Different deposition months cause annually integrated total runoff perturbation to
295 vary by 40-60% (12 Gt/yr in the maximum BC deposition case). Also, we find BC
296 deposition in June and July induces the largest annually integrated total runoff
297 increase. To further verify the most influential deposition month, we select five wet
298 BC and five dry BC deposition values, and plot total runoff increase versus
299 deposition month, shown in Figure 14. Figure 14a shows annual integrated total
300 runoff from the base run, starting from different months, serving as a reference for
301 the perturbations shown in Figure 14b-f. For different deposition amounts from low
302 to high (Figure 14b-f), BC deposition in summer (i.e., June, July and August) causes
303 the highest annual total runoff increase. With higher deposition (Figure 14e-f), June

304 deposition generates the largest annual total runoff for both dry and wet BC
305 deposition, whereas with lower deposition amounts the month of maximum impact
306 can be June or July. As noted earlier, however, deposition during non-summer
307 months also causes substantial melt and runoff perturbations, owing to the melt-
308 induced re-surfacing of impurities during summer in the ablation zone.

309 **4 Evaluation and application of the kernel product**

310 We turn now to evaluating the kernel product and advising a straightforward
311 way in which it can be applied to realistic aerosol deposition fluxes. We perform ten
312 one-year CLM simulations with spatially and temporally-varying wet or dry BC
313 deposition fluxes occurring in randomly selected years and months, and we evaluate
314 the accuracy of the kernel product using total GrIS BC deposition amount and total
315 runoff from these new simulations (the "evaluating simulations"), compared with
316 total runoff from the kernel for equivalent deposition fluxes. The evaluating
317 simulations use prescribed wet and dry BC deposition fields that were generated
318 from a global aerosol run with CAM (Lamarque et al., 2010). In different evaluating
319 simulations, the prescribed BC deposition fields are multiplied by factors ranging
320 from 2-50 for wet BC deposition and 2000-20000 for dry BC deposition to provide
321 different BC deposition amounts within the range of wet or dry deposition in the
322 kernel. High scaling factors are applied to dry/hydrophobic BC deposition
323 simulations because the prescribed dry BC deposition from CAM is very low and
324 within the noise regime. We also perform two ten-year (2006-2015) evaluating
325 simulations with both CAM prescribed wet and dry BC deposition fluxes turned on

326 throughout the whole simulations, to examine short-term, long-term and
327 climatological one-year integrated total runoff effects. BC deposition fluxes in one of
328 the ten-year evaluating simulations are multiplied by a factor of 5 to provide a high
329 deposition event and are left at unperturbed (i.e., realistic) values in the other
330 simulation. Also, different deposition years and months indicate different BC
331 distributions. Therefore, the evaluating simulations provide a variety of scenarios
332 with distinct BC deposition amounts and distributions to evaluate performance of
333 the kernel.

334 Figure 15 shows maximum, mean and minimum one-year integrated total
335 runoff increase versus BC deposition amount from the kernel product, with results
336 from the evaluating simulations overlaid on the kernel lines. With varying BC
337 deposition amount and distribution, including with combined wet and dry BC
338 deposition fluxes, results from the evaluating simulations are mostly within the total
339 runoff ranges of our kernel product for both wet and dry BC deposition. In the
340 evaluating simulations with combined wet and dry BC depositions, hydrophobic BC
341 fluxes are very low (<1/100 of wet BC fluxes), therefore, we treat all BC deposition
342 as wet/hydrophilic BC, and overlay the results on the wet deposition curves. We
343 note CAM simulated BC deposition from the 1 time evaluating run is comparable
344 with measured values of BC in Greenland snow and ice core measurements
345 (Polashenski et al., 2015; McConnell et al., 2007). The increases of one-year
346 integrated total runoff from the ten-year evaluating simulations with realistic
347 deposition exhibit wide ranges, for example, with a minimum of ~4 Gt in the first
348 deposition year (2006) to a maximum of ~10 Gt, and with a minimum of ~14 Gt in

349 the first year to a maximum of ~40 Gt in the simulation with 5 times BC fluxes. The
350 climatological (i.e., averaged over 10 years) total runoff perturbations (~8 Gt/yr and
351 ~30 Gt/yr in the default and 5 times simulations, respectively) caused by prescribed
352 combined wet and dry BC deposition are about double the first-year total runoff
353 integrations, which is due to continuous month by month depositions in the ten-
354 year evaluating simulations and the long-term effects of the reappearance of
355 residual BC at the surface as described in section 2.2.

356 Because the mean and maximum kernel curves in Figure 15 provide estimates
357 of BC induced total runoff within a reasonable range, we parameterize these curves
358 to provide a simple application of our kernel product. GrIS-wide melt perturbations
359 are relatively linear with BC deposition amount, with linear fits to the mean kernel
360 curves for wet and dry BC deposition fluxes of, respectively:

361 $$\Delta TOTALRUNOFF = 4.498e5 * \Delta wetBC, \quad (1)$$

362 $$\Delta TOTALRUNOFF = 3.062e5 * \Delta dryBC, \quad (2)$$

363 and with linear fits to the maximum kernel curves of:

364 $$\Delta TOTALRUNOFF\_MAX = 9.322e5 * \Delta wetBC, \quad (3)$$

365 $$\Delta TOTALRUNOFF\_MAX = 6.348e5 * \Delta dryBC, \quad (4)$$

366 where ΔTOTALRUNOFF is the mean increase in one-year integrated total runoff (kg
367 yr^{-1}), ΔTOTALRUNOFF_MAX is the maximum increase in one-year integrated total
368 runoff (kg yr^{-1}), and ΔwetBC and ΔdryBC are total wet and dry BC deposition fluxes
369 to the GrIS (kg yr^{-1}). Unique relationships for wet and dry deposition arise, again,
370 because of differences in optical properties and melt-induced removal efficiencies of
371 hydrophilic and hydrophobic BC. Linearity in the relationship between runoff and

BC deposition is encouraging because we have neglected coincident darkening from other types of LAI (e.g., dust, algae). In environments where darkening from other LAI is not too great, the runoff–BC relationships derived here should be valid, though we acknowledge that the incremental effect of BC will be lower in snow that is heavily laden with other impurities.

The bulk relationships shown above represent the simplest application of our kernel product, allowing a rough estimation of runoff perturbation caused by Greenland-wide wet and dry BC deposition fluxes. Based on the evaluations in Figure 15, the mean curves (i.e., equations (1) and (2)) from the kernel product tend to provide a conservative estimate of total runoff, whereas the maximum curves (i.e., equations (3) and (4)) represent a more realistic approximation of total runoff induced by BC deposition that occurs continuously and with varying spatial distribution. Ideally, gridcell-by-gridcell fluxes should be matched to the kernel to account for spatial differences in melt associated with elevation and other conditions (Figure 11 and Figure 12), but at the low end of deposition flux we see considerable noise at the individual pixel and deposition month level, especially for wet deposition fluxes that can be subject to anomalies associated with low precipitation amounts in a given month. To ameliorate this, for typical present-day deposition fluxes we recommend matching month-specific, but spatially-integrated deposition fluxes or concentrations with the associated Greenland-wide kernel values. Given the large uncertainties that exist in the bulk relationships, even as simulated with complex models, simple parameterizations that include large error bounds are justifiable and will facilitate more analyses of the extended impacts of

aerosol deposition to the GrIS.

Finally, although this product only includes BC, we suggest that it could be extended to include other LAI species through a simple scaling that accounts for the ratio of mass-specific absorption between the species of interest and the BC explored here. Rationale for this is that radiative forcing and melt perturbation will scale roughly linearly with absorptivity, at least for relatively low and moderate burdens of LAI. The mass-specific visible band absorption cross-sections assumed in our study for hydrophilic (via wet deposition) and hydrophobic (via dry deposition) BC are 7.5 and 11.3 $m^2\ g^{-1}$, respectively. The only other species-specific property affecting results from this study is the meltwater scavenging coefficient, which is assumed to be 0.2 for hydrophilic BC and 0.03 for hydrophobic BC (Flanner et al., 2007). Given relatively large uncertainty in this parameter (Doherty et al., 2013; Qian et al., 2014), we suggest applying the hydrophilic (wet deposition) kernel to all hydrophilic species and the hydrophobic (dry deposition) kernel to all hydrophobic species, along with appropriate scaling of optical properties.

5 Conclusions

In this study, ~6,000 simulations are performed to investigate annually integrated runoff perturbation from BC deposition on snow. The simulation matrix includes variations in deposition flux, deposition month and year, and nature of the deposition (wet or dry). From this matrix we produce a large-ensemble kernel that relates BC deposition fluxes to GrIS runoff perturbations.

In the month after deposition, top-snow layer BC concentration decreases

417 rapidly due to fresh snow coverage, but then increases somewhat in the ablation
418 zone during the following summer due to melt-induced re-exposure of the
419 contaminated snow. Accordingly, the total runoff increase induced by BC deposition
420 is substantial for both summer and winter deposition, though with peak impacts
421 associated with June and July deposition. Impacts from winter deposition suggest
422 that winter emissions, associated for example with biomass heating use, should not
423 be neglected as potential contributors to increased summer melt. Also, we find most
424 of the runoff increase occurs along the margins, and especially on the southern
425 margin of Greenland, with little sign of melting in the center of the GrIS where it is
426 rarely warm enough. Inter-annual variations in total runoff in the base and BC
427 perturbed simulations indicate that BC deposition can generate more impact in
428 warmer years, when more of the ice surface is near the melting temperature.
429 In summary, higher BC deposition amount leads to higher total runoff. We do
430 not find a clear sign of runoff saturation caused by high BC deposition values in our
431 study. Model-generated deposition fluxes associated with realistic BC emissions
432 induce a climatological-mean (2006-2015) GrIS-wide runoff increase of 8 Gt/yr
433 (+6.8% perturbation), which corresponds to 0.022 mm/year of global sea level rise.
434 We also suggest simple, linear equations that crudely relate GrIS-wide wet and dry
435 BC deposition fluxes to annually-integrated runoff perturbation, and provide links
436 to the full spatially-varying kernel dataset so that users can derive more accurate
437 estimates of melt perturbation (e.g., resolved by seasonal timing) from deposition
438 fluxes. We also suggest that the kernel results can be applied to other LAI species
439 via simple scaling of the mass absorption cross-section. Our hope is that these data

will extend the utility of state-of-the-art aerosol models.

Acknowledgments

This research was supported by the Department of Energy (DOE) grant DE-SC0013991. The kernel product from model runs in this paper have been archived by the corresponding author, Yang Li (University of Michigan; yanglibj@umich.edu), and are available upon request through e-mail.

References

Bond, T. C., Bhardwaj, E., Dong, R., Jogani, R., Jung, S., Roden, C., Streets, D. G., and Trautmann, N. M.: Historical emissions of black and organic carbon aerosol from energy-related combustion, 1850–2000, Global Biogeochemical Cycles, 21, n/a-n/a, 10.1029/2006GB002840, 2007.

Bond, T. C., Doherty, S. J., Fahey, D. W., Forster, P. M., Berntsen, T., DeAngelo, B. J., Flanner, M. G., Ghan, S., Kärcher, B., Koch, D., Kinne, S., Kondo, Y., Quinn, P. K., Sarofim, M. C., Schultz, M. G., Schulz, M., Venkataraman, C., Zhang, H., Zhang, S., Bellouin, N., Guttikunda, S. K., Hopke, P. K., Jacobson, M. Z., Kaiser, J. W., Klimont, Z., Lohmann, U., Schwarz, J. P., Shindell, D., Storelvmo, T., Warren, S. G., and Zender, C. S.: Bounding the role of black carbon in the climate system: A scientific assessment, Journal of Geophysical Research: Atmospheres, 118, 5380-5552, 10.1002/jgrd.50171, 2013.

Box, J., Fettweis, X., Stroeve, J., Tedesco, M., Hall, D., and Steffen, K.: Greenland ice sheet albedo feedback: thermodynamics and atmospheric drivers, The Cryosphere, 6, 821-839, 2012.

Doherty, S., Warren, S., Grenfell, T., Clarke, A., and Brandt, R.: Light-absorbing impurities in Arctic snow, Atmospheric Chemistry and Physics, 10, 11647-11680, 2010.

Doherty, S. J., Grenfell, T. C., Forsström, S., Hegg, D. L., Brandt, R. E., and Warren, S. G.: Observed vertical redistribution of black carbon and other insoluble light‐absorbing particles in melting snow, Journal of Geophysical Research: Atmospheres, 118, 5553-5569, 2013.

Dumont, M., Brun, E., Picard, G., Michou, M., Libois, Q., Petit, J. R., Geyer, M., Morin, S., and Josse, B.: Contribution of light-absorbing impurities in snow to Greenland's darkening since 2009, Nature Geoscience, 7, 509, 10.1038/ngeo2180 https://www.nature.com/articles/ngeo2180#supplementary-information, 2014.

Flanner, M. G., Zender, C. S., Randerson, J. T., and Rasch, P. J.: Present-day climate forcing and response from black carbon in snow, Journal of Geophysical Research: Atmospheres, 112, n/a-n/a, 10.1029/2006JD008003, 2007.

Flanner, M. G., Zender, C. S., Hess, P. G., Mahowald, N. M., Painter, T. H., Ramanathan, V., and Rasch, P.: Springtime warming and reduced snow cover from carbonaceous particles, Atmospheric Chemistry and Physics, 9, 2481-2497, 2009.

Hansen, J., and Nazarenko, L.: Soot climate forcing via snow and ice albedos, Proceedings of the National Academy of Sciences of the United States of America, 101, 423-428, 2004.

Hansen, J. e., Sato, M., Ruedy, R., Nazarenko, L., Lacis, A., Schmidt, G., Russell, G., Aleinov, I., Bauer, M., and Bauer, S.: Efficacy of climate forcings, Journal of Geophysical Research: Atmospheres, 110, 2005.

Jacobson, M. Z.: Climate response of fossil fuel and biofuel soot, accounting for soot's feedback to snow and sea ice albedo and emissivity, Journal of Geophysical Research: Atmospheres, 109, 2004.
Jiao, C., Flanner, M., Balkanski, Y., Bauer, S., Bellouin, N., Berntsen, T., Bian, H., Carslaw, K., Chin, M., and De Luca, N.: An AeroCom assessment of black carbon in Arctic snow and sea ice, Atmospheric Chemistry and Physics, 14, 2399-2417, 2014.
Jordan, R.: A one-dimensional temperature model for a snow cover: Technical documentation for SNTHERM. 89, COLD REGIONS RESEARCH AND ENGINEERING LAB HANOVER NH, 1991.
Keegan, K. M., Albert, M. R., McConnell, J. R., and Baker, I.: Climate change and forest fires synergistically drive widespread melt events of the Greenland Ice Sheet, Proceedings of the National Academy of Sciences, 111, 7964-7967, 2014.
Kintisch, E.: Meltdown, in, American Association for the Advancement of Science, 2017.
Krabill, W., Hanna, E., Huybrechts, P., Abdalati, W., Cappelen, J., Csatho, B., Frederick, E., Manizade, S., Martin, C., and Sonntag, J.: Greenland ice sheet: increased coastal thinning, Geophysical Research Letters, 31, 2004.
Lamarque, J.-F., Bond, T. C., Eyring, V., Granier, C., Heil, A., Klimont, Z., Lee, D., Liousse, C., Mieville, A., and Owen, B.: Historical (1850–2000) gridded anthropogenic and biomass burning emissions of reactive gases and aerosols: methodology and application, Atmospheric Chemistry and Physics, 10, 7017-7039, 2010.
McConnell, J. R., Edwards, R., Kok, G. L., Flanner, M. G., Zender, C. S., Saltzman, E. S., Banta, J. R., Pasteris, D. R., Carter, M. M., and Kahl, J. D.: 20th-century industrial black carbon emissions altered arctic climate forcing, Science, 317, 1381-1384, 2007.
Oleson, K., Lawrence, M., Bonan, B., Drewniak, B., Huang, M., Koven, D., Levis, S., Li, F., Riley, J., and Subin, M.: Technical description of version 4.5 of the Community Land Model (CLM), 2013.
Polashenski, C. M., Dibb, J. E., Flanner, M. G., Chen, J. Y., Courville, Z. R., Lai, A. M., Schauer, J. J., Shafer, M. M., and Bergin, M.: Neither dust nor black carbon causing apparent albedo decline in Greenland's dry snow zone: Implications for MODIS C5 surface reflectance, Geophysical Research Letters, 42, 9319-9327, 2015.
Qian, Y., Wang, H., Zhang, R., Flanner, M. G., and Rasch, P. J.: A sensitivity study on modeling black carbon in snow and its radiative forcing over the Arctic and Northern China, Environmental Research Letters, 9, 064001, 2014.
Rignot, E., and Kanagaratnam, P.: Changes in the velocity structure of the Greenland Ice Sheet, Science, 311, 986-990, 2006.
Rignot, E., Velicogna, I., van den Broeke, M. R., Monaghan, A., and Lenaerts, J. T.: Acceleration of the contribution of the Greenland and Antarctic ice sheets to sea level rise, Geophysical Research Letters, 38, 2011.
Shepherd, A., Ivins, E. R., Geruo, A., Barletta, V. R., Bentley, M. J., Bettadpur, S., Briggs, K. H., Bromwich, D. H., Forsberg, R., and Galin, N.: A reconciled estimate of ice-sheet mass balance, Science, 338, 1183-1189, 2012.

Shimada, R., Takeuchi, N., and Aoki, T.: Inter-annual and geographical variations in the extent of bare ice and dark ice on the Greenland ice sheet derived from MODIS satellite images, Frontiers in Earth Science, 4, 43, 2016.

Tedesco, M.: Snowmelt detection over the Greenland ice sheet from SSM/I brightness temperature daily variations, Geophysical Research Letters, 34, 2007.

Tedesco, M., Doherty, S., Fettweis, X., Alexander, P., Jeyaratnam, J., and Stroeve, J.: The darkening of the Greenland ice sheet: trends, drivers, and projections (1981–2100), Cryosphere (The), 10, 477-496, 2016.

Thomas, J. L., Polashenski, C. M., Soja, A. J., Marelle, L., Casey, K., Choi, H. D., Raut, J. C., Wiedinmyer, C., Emmons, L. K., and Fast, J.: Quantifying black carbon deposition over the Greenland ice sheet from forest fires in Canada, Geophysical Research Letters, 2017.

van den Broeke, M., Bamber, J., Ettema, J., Rignot, E., Schrama, E., van de Berg, W. J., van Meijgaard, E., Velicogna, I., and Wouters, B.: Partitioning recent Greenland mass loss, science, 326, 984-986, 2009.

Vaughan, D. G., Comiso, J. C., Allison, I., Carrasco, J., Kaser, G., Kwok, R., Mote, P., Murray, T., Paul, F., and Ren, J.: Observations: cryosphere, Climate change, 2103, 317-382, 2013.

Viovy, N.: CRU-NCEP Version 4, available at: http://dods.extra.cea.fr/data/p529viov/cruncep/V4_1901_2012/ last access: August 2012.

Zwally, H. J., Abdalati, W., Herring, T., Larson, K., Saba, J., and Steffen, K.: Surface melt-induced acceleration of Greenland ice-sheet flow, Science, 297, 218-222, 2002.

558 **Figure Captions**

559

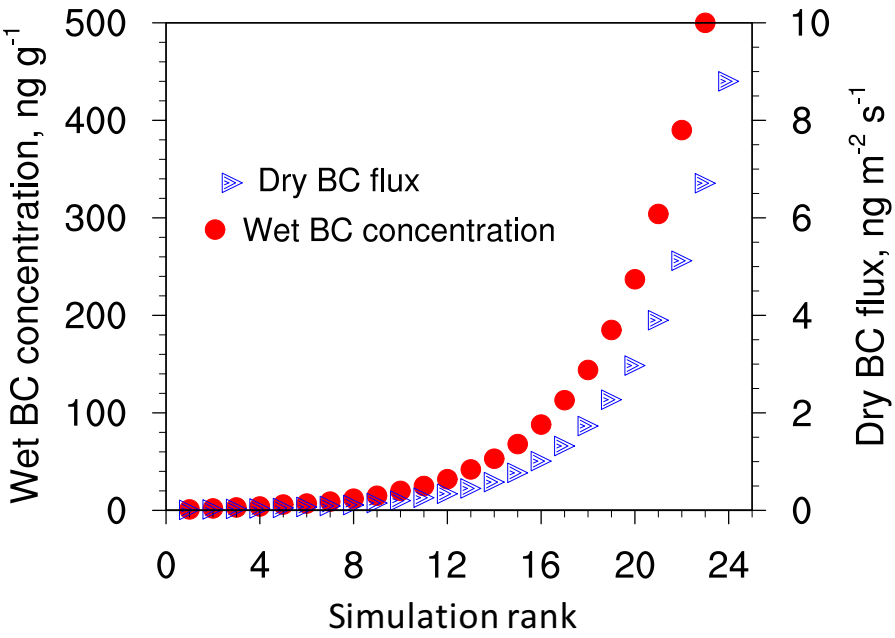

560

561 **Figure 1.** Prescribed values of BC concentrations in precipitation (red) and dry

562 deposition fluxes (blue) applied in the CESM modeling studies. Spacing between

563 values is logarithmic.

564

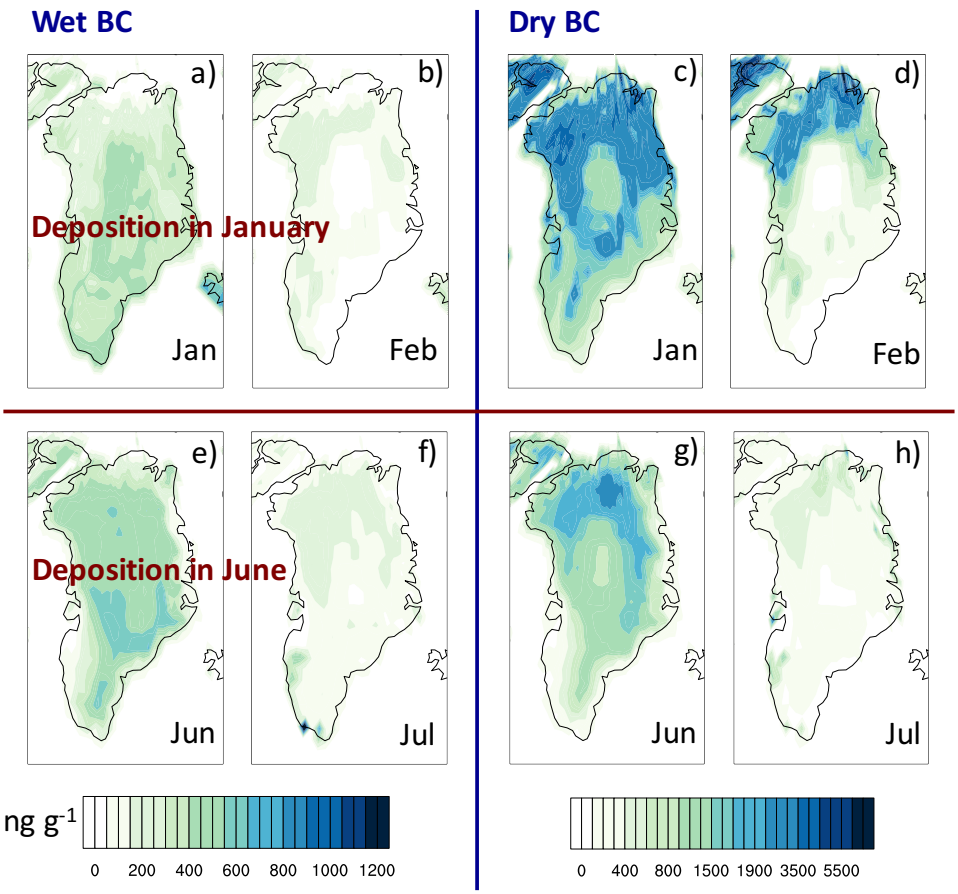

565

566 **Figure 2.** Ten-year (2006-2015) averaged hydrophilic BC concentration associated
567 with wet deposition (a, b, e, f) and hydrophobic BC concentration associated with
568 dry deposition (c, d, g, h) in the top snow layer. The contour maps show
569 concentrations caused by January deposition (a-d) and June deposition (e-h),
570 associated with the maximum wet and dry deposition scenarios depicted in Figure
571 1.

572

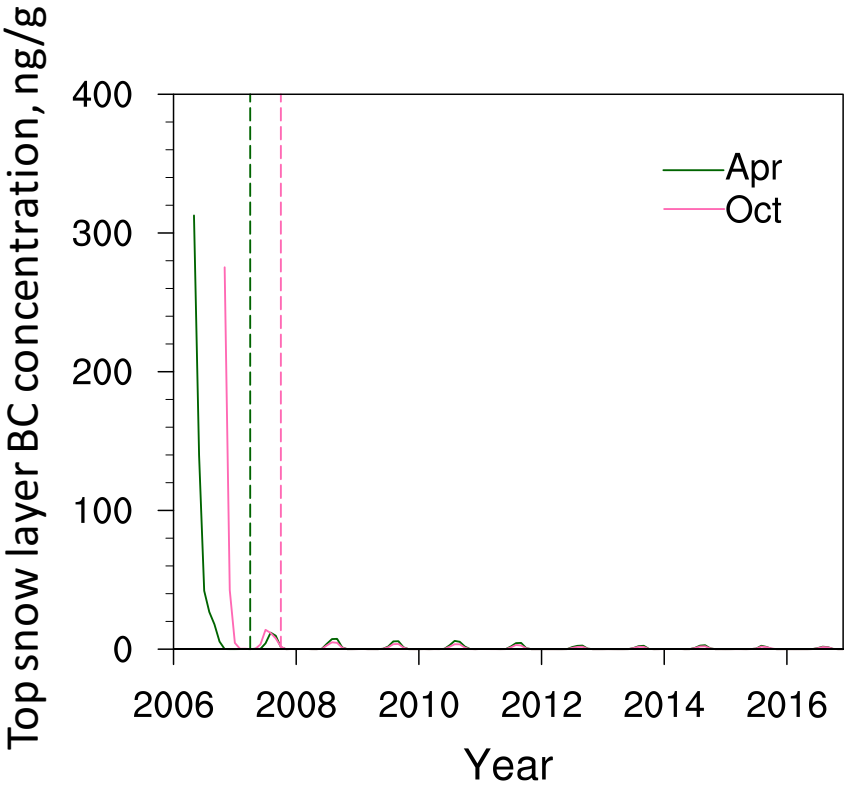

573

574 **Figure 3.** Temporal evolution of hydrophilic BC concentration in the top snow layer
575 averaged over the Greenland region from two 11-year (2006-2016) simulations
576 with wet BC deposition occurring in April and October of the first year. The BC
577 concentration in precipitation is the maximum value shown in Figure 1. Dashed
578 lines represent the ends of one year since different deposition months.

579

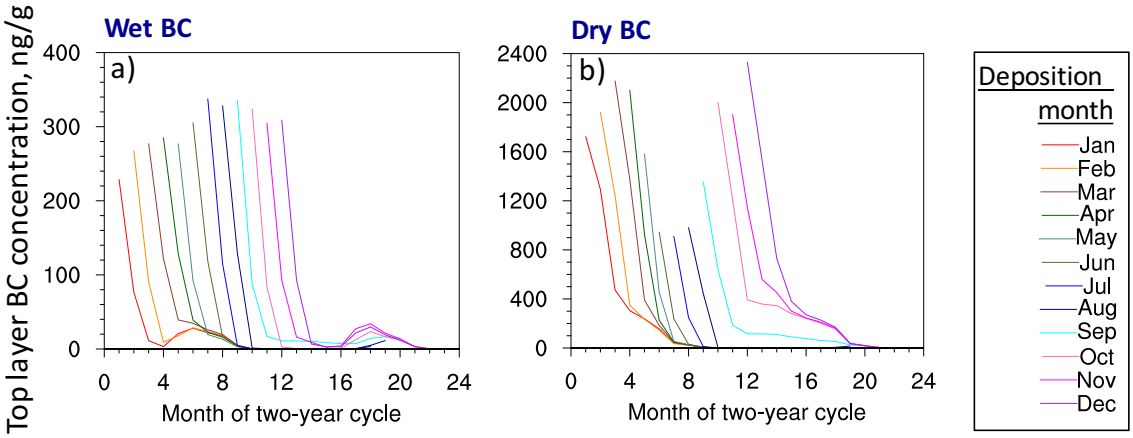

580

581 **Figure 4.** Temporal evolution of hydrophilic BC concentration (a) and hydrophobic

582 BC concentration (b) in the top snow layer averaged over the Greenland region from

583 the simulations with the maximum wet and dry BC deposition, respectively. Each

584 line starts from the BC deposition month, extends one year, and represents the

585 mean time series from 10 simulations that start in each year from 2006-2015.

586

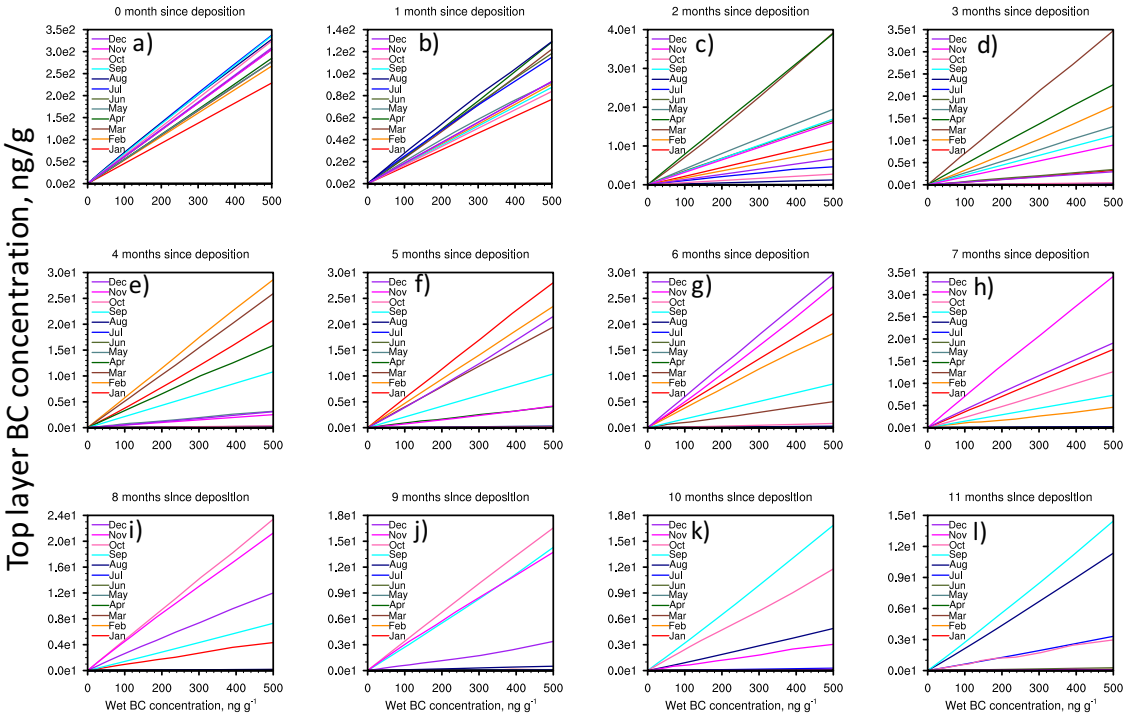

587

588 **Figure 5.** Hydrophilic BC concentration in the top snow layer vs. concentration of

589 BC in precipitation shown at different times (0-11 months, panels a-l) since

590 deposition. The top-snow layer concentrations are averaged over the Greenland

591 region and over ten one-year simulations beginning in years 2006-2015. Different

592 line colors represent different deposition months.

593

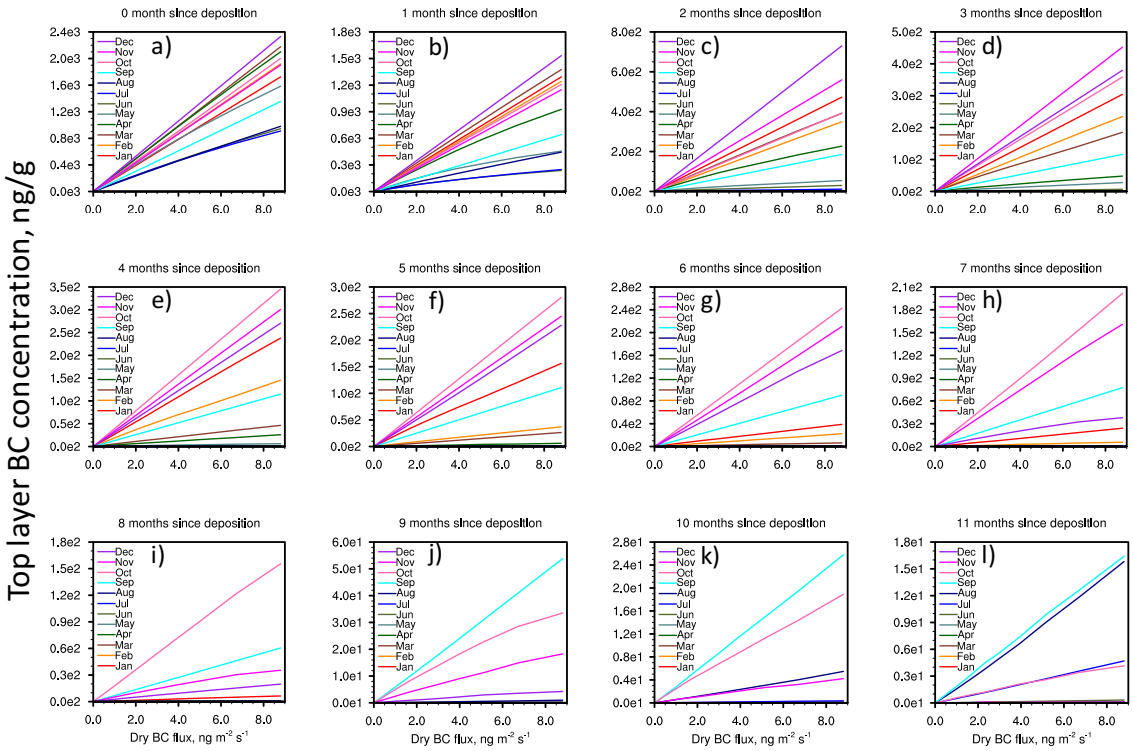

Figure 6. Same as Figure 5, but showing hydrophobic BC concentration in the top snow layer vs. BC dry deposition flux.

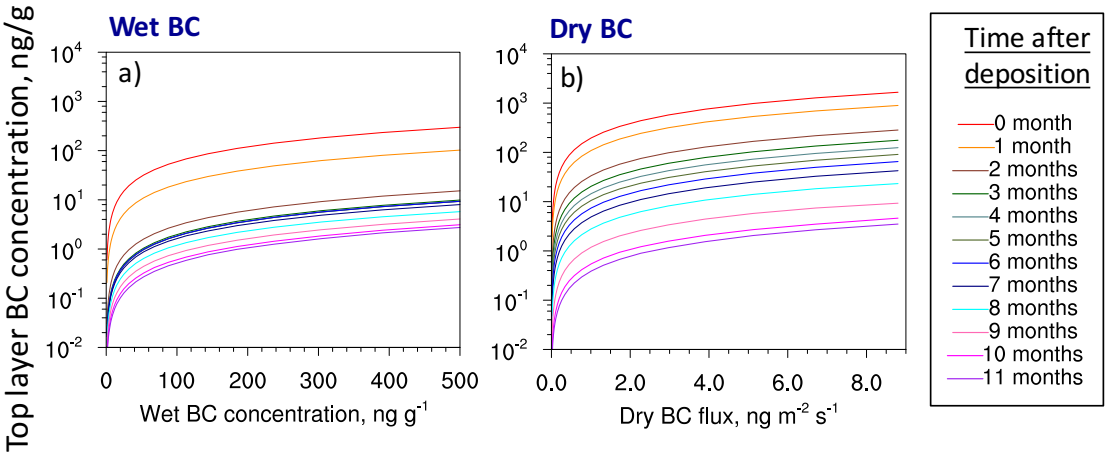

602

603 **Figure 7.** Hydrophilic BC concentration in the top snow layer vs. concentration of

604 BC in precipitation (a), and hydrophobic BC concentration in the top snow layer vs.

605 BC dry deposition flux (b) shown at different times (0-11 months) since deposition.

606 The top-snow layer concentrations are averaged over the Greenland region, over all

607 the deposition months and over ten one-year simulations beginning in years 2006-

608 2015.

609

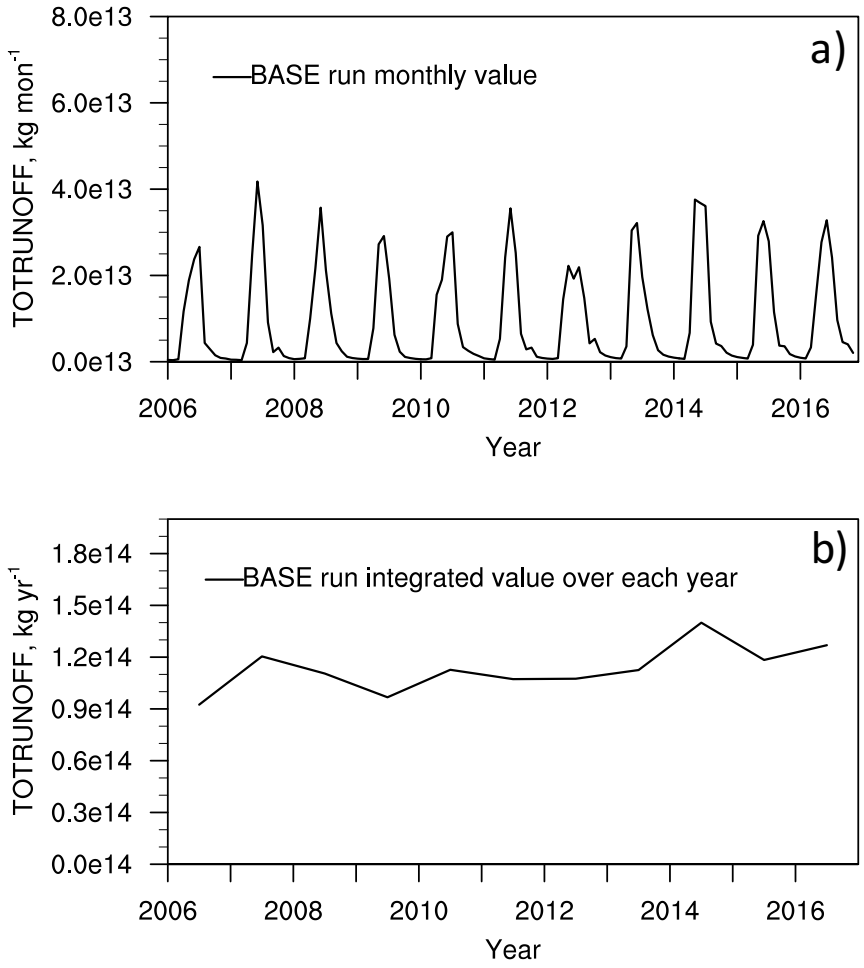

610

611 **Figure 8.** Monthly (a) and annually integrated (b) timeseries of total runoff from

612 Greenland in the Base run without BC deposition.

613

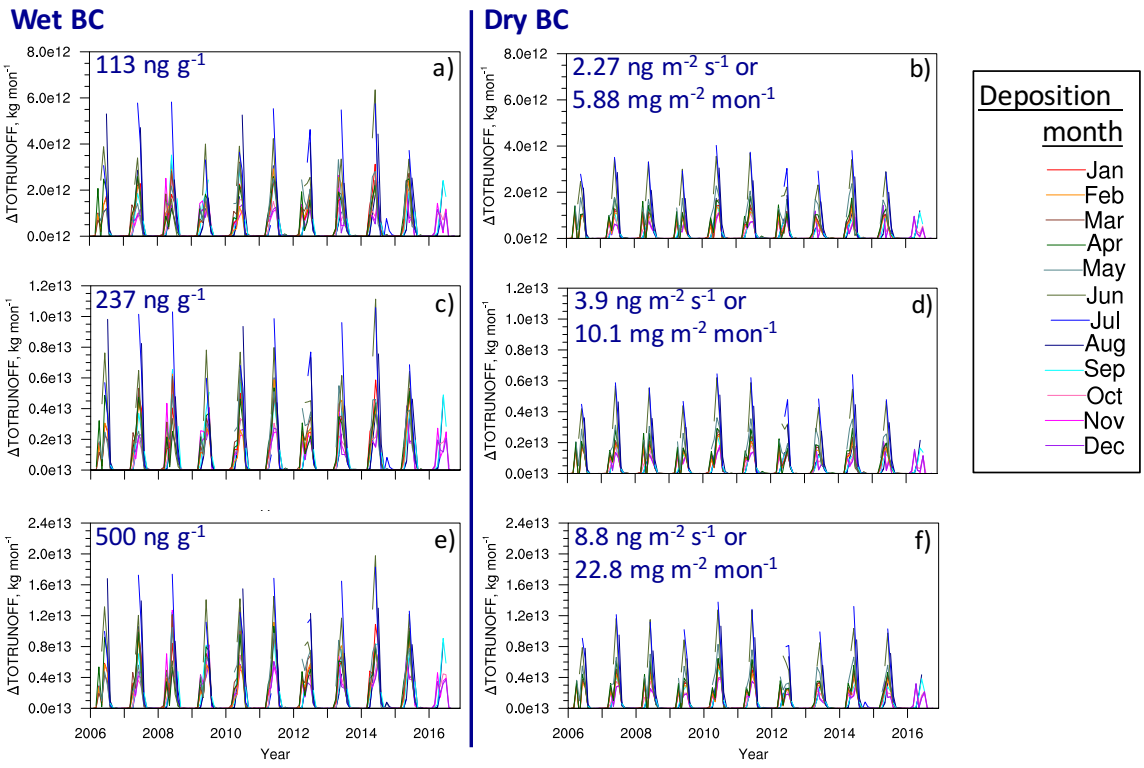

614

615 **Figure 9.** Monthly timeseries of the increase in total Greenland runoff resulting

616 from BC deposition. Values of BC concentrations in precipitation (a, c, e) and dry

617 deposition fluxes (b, d, f) are shown in each plot. Each line starts from the BC

618 deposition month and extends one year. Different line colors represent different

619 deposition months.

620

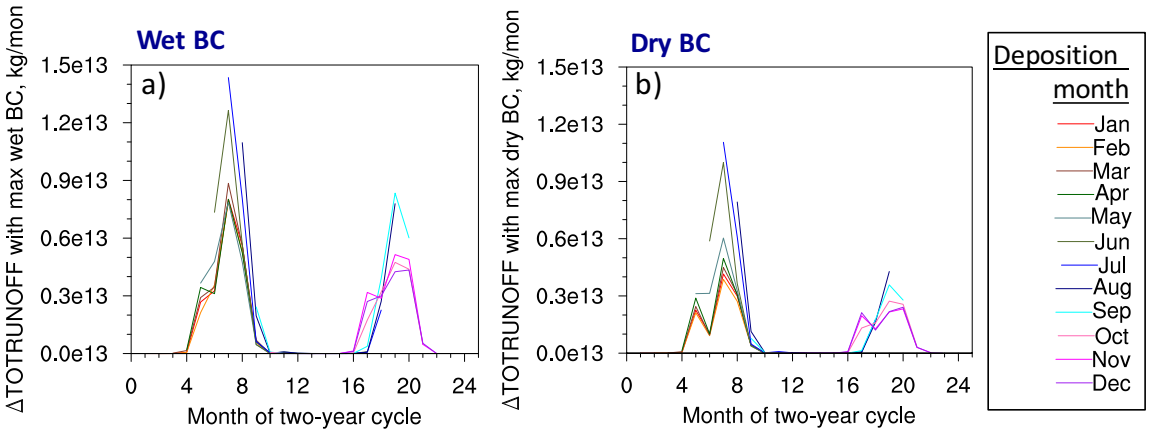

621

622 **Figure 10.** Temporal evolution of ten-year (2006-2015) averaged total runoff

623 increase resulting from BC deposition, summed over the entire Greenland region

624 from the simulations with the maximum wet (a) and dry (b) BC deposition. Each line

625 starts from the BC deposition month and extends one year.

626

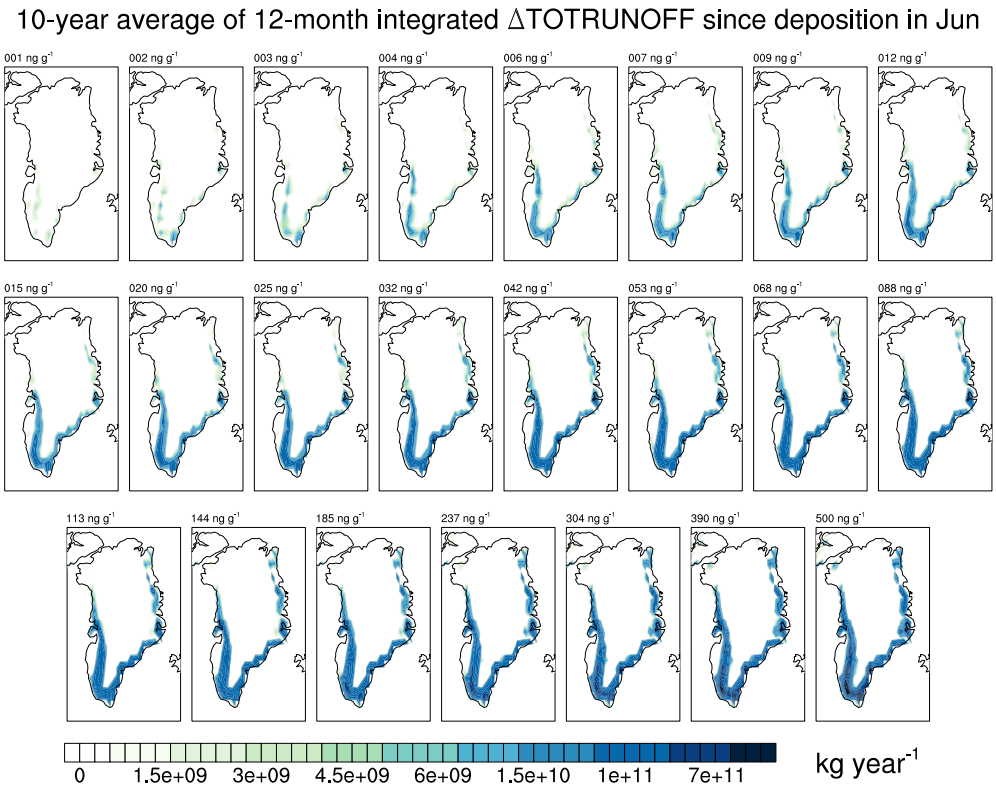

627

628 **Figure 11.** Ten-year average of annually-integrated total runoff increase resulting

629 from different concentrations of BC in precipitation, deposited only during June.

630 The average is over ten one-year simulations starting in each year from 2006-2015.

631

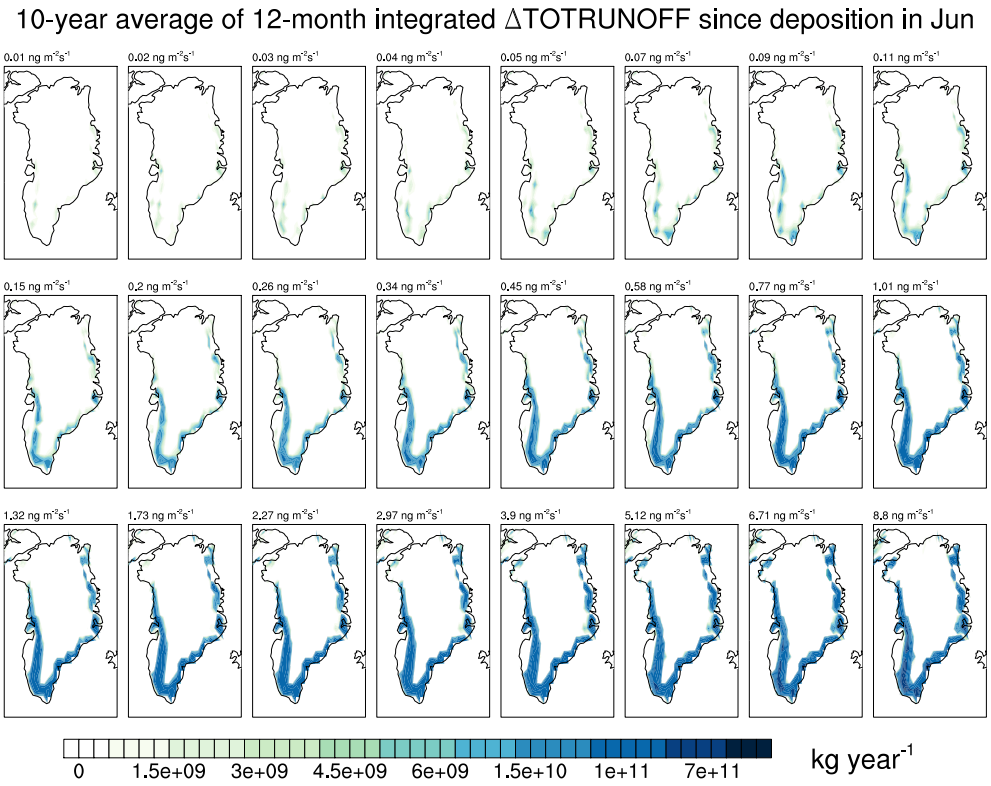

632

633 **Figure 12.** Same as Figure 11, but resulting from different dry deposition fluxes of

634 BC in June.

635

636

637

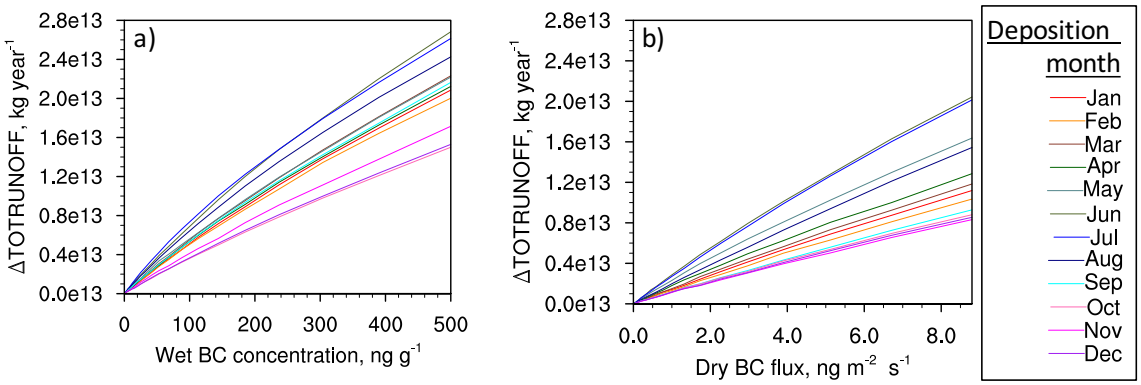

638

639 **Figure 13.** Increase in total Greenland runoff resulting from BC deposition

640 integrated over one year starting from the month of BC deposition vs. concentration

641 of BC in precipitation (a) and vs. BC dry deposition flux (b). The runoff values are

642 summed over the Greenland region and averaged over ten one-year simulations

643 beginning in years 2006-2015. Different line colors represent different deposition

644 months.

645

646

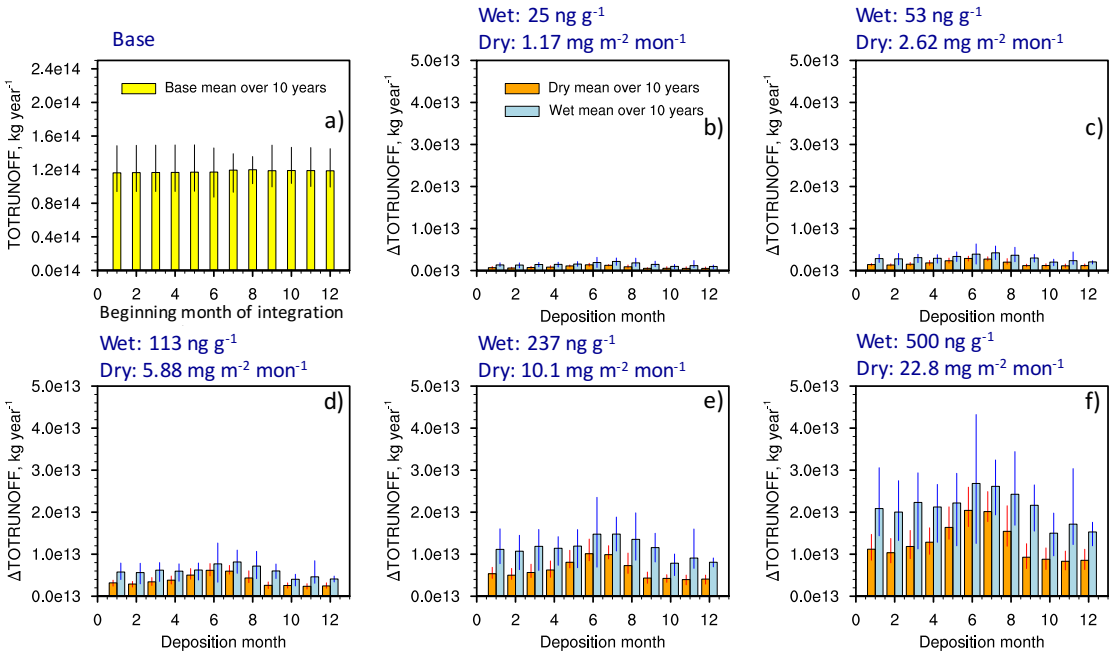

647

648 **Figure 14.** Total runoff in the Base run without BC deposition (a) and the increase
649 in total Greenland runoff resulting from BC deposition (b-f), integrated over one
650 year starting from the month of BC deposition. The bars show mean values and the
651 whiskers depict the full range of values over all ten simulations that each start in a
652 different year from 2005-2016. Values of BC concentrations in precipitation and dry
653 deposition fluxes are shown in the title of each plot (b-f).

654

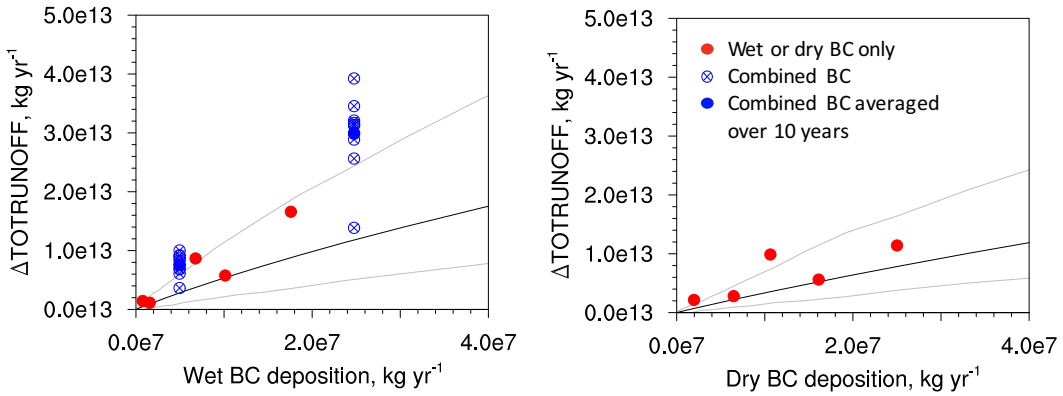

655

656 **Figure 15.** Increase in total Greenland runoff resulting from BC deposition
657 integrated over one year starting from the month of BC deposition vs. total wet (a)
658 and dry (b) BC deposition mass flux over the entire GrIS. The runoff values are
659 summed over the Greenland region and averaged over all deposition years and
660 deposition months. Black lines show mean total runoff values, and grey lines show
661 maximum and minimum values from the entire matrix of simulations. Red dots
662 represent explicitly-simulated total runoff from the evaluating simulations with
663 prescribed spatially and temporally-varying wet or dry BC deposition fluxes in
664 randomly selected months and years. Blue hollow circles represent simulated total
665 runoff from the evaluating simulations with prescribed combined BC deposition
666 fluxes integrated over each year of the ten-year simulations. Blue dots show
667 averages of the hollow circles.

668